

Nucleation and Growth of Eutectic Si in Al-Si Alloys with Na Addition

J.H. LI, J. BARRIRERO, M. ENGSTLER, H. ABOULFADL, F. MÜCKLICH,
and P. SCHUMACHER

Al-5 wt pct Si-based alloys with Na additions (19 and 160 ppm) have been produced by controlled sand casting and melt spinning. Entrained droplet technique and differential scanning calorimetry were employed to investigate the nucleation behavior of eutectic Si. High-resolution transmission electron microscopy and atom probe tomography were used to investigate the distribution of Na atoms within eutectic Si and at the interfaces between eutectic Si and eutectic Al. It was found that (i) only 19 ppm Na addition results into a high undercooling (49 K (49 °C)) of the entrained eutectic droplet. However, further increasing Na addition up to 160 ppm exerts no positive effect on the nucleation of eutectic Si, instead a decreased undercooling (29 K (29 °C)) was observed. (ii) Na addition suppresses the growth of eutectic Si due to the Na segregation at the interface between eutectic Si and eutectic Al, and (iii) Na addition promotes significant multiple Si twins, which can be attributed to the proposed adsorption of Na atoms at the intersection of Si twins and along the $\langle 112 \rangle_{\text{Si}}$ growth direction of Si. The present investigation demonstrates, for the first time, a direct observation on the distribution of Na atoms within eutectic Si and thereby provides strong experimental supports to the well-accepted impurity-induced twinning growth mechanism and poisoning of the twin plane re-entrant edge growth mechanism.

DOI: 10.1007/s11661-014-2702-6

© The Minerals, Metals & Materials Society and ASM International 2014

I. INTRODUCTION

Na has been firstly used to modify the eutectic Si in Al-Si alloys since 1921.^[1] However, Na modification has been replaced, or is being reduced, by Sr modification due to the inherent disadvantages of Na modification, *i.e.*, evaporation, high volatility, rapid fade from the melt, and a tendency to overmodification.^[1] Compared with Sr modification, the effects of Na addition on the nucleation and growth of eutectic Si are still not fully understood due to the lack of a detailed experimental investigation on Na modification.

Similar to Sr modification, it is generally accepted that impurity-induced twinning (IIT) growth mechanism,^[2] twin plane re-entrant edge (TPRE) growth mechanism^[3,4] as well as poisoning of the TPRE^[5] are also valid for Na modification under certain conditions. The IIT mechanism postulates that the modifier can be adsorbed on the growing $\{111\}_{\text{Si}}$ planes producing frequent multiple Si twins. The TPRE mechanism proposes that Si growth occurs more readily at the re-

entrant edge along the $\langle 112 \rangle_{\text{Si}}$ growth direction of Si while poisoning of the TPRE assumes that the modifier retards the Si growth by selectively adsorbing at the TPRE, thus deactivating the growth advantage of the TPRE and forcing new growth of the TPRE. However, in contrast to detailed investigations on Sr modification,^[6–14] there is still a lack of, if any, detailed experimental investigations on the distribution of Na atoms within eutectic Si. This is mainly due to the very low Na content (less than 50 ppm) and the difficulties of Na observation within eutectic Si using scanning transmission electron microscopy (STEM) due to their very close Z atomic numbers ($Z_{\text{Na}} = 11$, $Z_{\text{Al}} = 13$, $Z_{\text{Si}} = 14$) and thereby the weak contrast in STEM high-angle annular dark field (HAADF) image.

It has been reported^[15] that Na atoms were adsorbed on $\{111\}_{\text{Si}}$ physically and homogeneously using X-ray photoelectron spectroscopy (XPS) and Auger electron spectroscopy (AES) analyses in hypereutectic Al-22 wt pct Si alloys with 0.25 and 0.6 wt pct Na additions. The existence of Na-enriched regions within primary Si crystals has also been reported in Al-16 wt pct Si alloy with Na addition using electron probe microanalysis (EPMA) and back-scattered electron images.^[16] Na-enriched regions were observed in narrow regions which spread from the center to the periphery of the multifaceted Si particle which appeared rounded in morphology. However, the distribution of Na atoms within eutectic Si has not been reported yet at an atomic scale. Therefore, in the case of Na modification, IIT, TPRE, or poisoning of the TPRE has not been supported experimentally.

J.H. LI, Senior Lecturer, is with the Institute of Casting Research, Montanuniversität Leoben, 8700 Leoben, Austria. Contact e-mail: jie-hua.li@hotmail.com J. BARRIRERO, M. ENGSTLER, and H. ABOULFADI, Doctoral Candidates, and F. MÜCKLICH, Professor, are with the Department of Materials Science, Saarland University, Campus D3.3, 66123 Saarbrücken, Germany. P. SCHUMACHER, Professor, is with the Institute of Casting Research, Montanuniversität Leoben, and also with the Austrian Foundry Research Institute, 8700 Leoben, Austria.

Manuscript submitted June 25, 2014.

Article published online December 12, 2014

In terms of the nucleation of eutectic Si, similar to Sr modification,^[6,17] the poisoning effect of Na modification on the AIP compound has also been reported by Mondolfo^[18] in hypoeutectic Al-Si alloys. Na addition was found to force the nucleation of Si to larger undercoolings. Similar results were also obtained by Ho and Cantor^[19] in hypoeutectic Al-Si alloys doped with different levels of P and Na using entrained droplet experiments. Adding Na (80 to 850 ppm) was found to lead to the formation of Na₃P in preference to AIP. It is the formation of Na₃P compound that reduces the amount of the potent AIP phase.^[20] Clearly, there is an important interaction between Na and AIP in Al-Si alloys. However, whether such type of interaction affects the growth of eutectic Si, and thereby the modification of eutectic Si is still not fully understood.

In the present investigation, the entrained droplet technique, which can be used to investigate the impurity effect on heterogeneous nucleation,^[6] was employed to investigate the nucleation of eutectic Si in Al-5 wt pct Si alloy with Na addition (19 and 160 ppm). In order to compare the observations under different solidification conditions, the samples produced using controlled sand casting and melt spinning were investigated using differential scanning calorimetry (DSC) and multi-scale microstructure characterization techniques from μm to sub-nm scales. In particular, high-resolution transmission electron microscopy (TEM) and atom probe tomography (APT) were used to investigate the distribution of Na atoms within eutectic Si and along the interfaces between eutectic Si and eutectic Al, with the aim to further elucidate the modification mechanism caused by Na addition.

II. EXPERIMENTAL METHODS

Al-5 wt pct Si alloys (wt pct, used throughout this paper unless otherwise noted) with and without Na addition were prepared, respectively, using high purity (HP) Al (5N, 99.998), HP Si chips (5N), and elemental Na (2N8, 99.8) supplied in vacuum-packed Al foils. The purity level of the used elemental Na is 2N8 (99.8). Other impurities (*i.e.*, Fe) may be also present. However, it can be expected that these possible impurities may have no significant effect on the nucleation and growth of eutectic Si because of the fact that the content of the possible impurities is very low (the Na content is about 19 and 160 ppm). The chemical concentration of Na was determined by inductively coupled plasma atomic emission spectrum (ICP-AES) apparatus. The chemical concentration of P, due to the Al and Si addition, even

with a high purity level, was determined with a Finnigan ELEMENT GD glow discharge mass spectrometer (GD-MS). Due to the fact that P comes from the Al and Si used, even with a high purity level (5N Al, 5N Si), repeated measurements (at least three times) of Al-5Si alloys with and without Na additions using GD-MS give a consistent value (about 0.44 ppm) if the used Al and Si remain the same impurity level, *i.e.*, 5N Al, 5N Si. Therefore, 0.44 ppm was used as an average P content.

The measured compositions of both alloys are given in Table I. The balance in Table I is Al. Although a trace Fe (about 10 ppm, coming from used Al and alloy melting and casting process) may be present, Fe has no significant effect on the nucleation and growth on eutectic Si, as reported in Reference 6.

In the case of controlled sand casting, experimental alloys were melted in an electric resistance furnace, and the temperature of the melt was kept at about 993 K (720 °C). Elemental Na in vacuum-packed Al foils was added before casting. No degassing was performed prior to casting. At least two samples for each condition were taken to perform thermal analysis using a Quik-Cup method in resin bounded sand molds. The dimensions of Quik-Cup are about 30 mm in length, 30 mm in width, and 30 mm in height. The average cooling rate is about 20 K min⁻¹ (20 °C min⁻¹), which is very close to the conventional sand casting even with a larger scale. Please note that the sample prepared using controlled sand casting method is in contrast to the work by Ho and Cantor,^[19] where the samples were prepared using arc melting.

In the case of melt spinning, two Na-containing alloys (about 15 g) were re-melted under high vacuum conditions and ejected onto a rotating copper wheel (20 m s⁻¹). A power-compensated PerkinElmer PYRIS Diamond DSC under an Ar atmosphere was used to measure the entrained droplet undercooling with a constant heating from 673 K to 873 K (400 °C to 600 °C), holding for 1 minute at 873 K (600 °C), and subsequent cooling to 673 K (400 °C) with a rate of 10 K min⁻¹ (10 °C min⁻¹). At least two DSC measurements (about 8 mg) were performed. Note that only the cooling curves were used to measure the entrained droplet undercooling because the instrument (DSC) calibration was performed during the cooling stage. For comparison, a similar DSC measurement was also performed for the controlled sand cast alloys.

Optical microscopy (OM), TEM, and APT were employed to characterize the as-cast microstructure in Al-5Si alloy with Na addition (19 and 160 ppm, Table I). Samples were taken from the center parts at the vicinity of the thermal couple. The specimens for

Table I. The Measured Compositions of Al-5Si-Based Alloy with Na Addition (wt pct)

Alloys	Elements			
	Si	Na (ppm)	P (ppm)	Al
Alloy 1	5.00	—	0.44	balance
Alloy 2	5.00	19	0.44	balance
Alloy 3	5.00	160	0.44	balance

OM investigation were mechanically ground, polished, and then etched using a mixture of 13 g boric acid, 35 g HF, and 800 ml H₂O. The specimens (ribbons in the melt spun condition and bulk samples in the controlled sand casting condition) for TEM investigation were mechanically ground, polished, and dimpled to about 30 μm, and then ion beam milled using a Gatan Precision Ion Polishing System (PIPS, Gatan model 691). During PIPS, the sample was cooled to about 253 K (−20 °C) and rotated with a speed of 3 r min^{−1}. Double guns with an accelerating voltage of about 4 kV and an angle of about +4 deg (left or right) and −4 deg (the other side) were used. TEM was performed using a Philips CM12 microscopy operated at 120 kV and an image-side Cs-corrected JEOL-2100F operated at 200 kV.

Sample preparation for APT (bulk samples produced by controlled sand casting) was performed in a dual-beam focused ion beam/scanning electron microscopy workstation (FIB/SEM) (Helios NanoLab 600™, FEI Company, USA) by the standard lift-out technique.^[21] After thinning of the samples, a low energy milling at 2 kV was performed to minimize the possible damage induced by Ga. APT was carried out in a LEAP™ 3000X HR (CAMECA). Specimens containing only eutectic Si were measured in laser-assisted mode with a pulse energy of 0.5 nJ and a repetition rate of 160 kHz. Specimens containing both eutectic Si and eutectic Al were measured in voltage mode at a pulse fraction of

20 pct and a repetition rate of 200 kHz. A specimen temperature of about 40 K, a pressure lower than 1×10^{-10} Torr (1.33×10^{-8} Pa), and an evaporation rate of 5 atoms per 1000 pulses were used for all measurements. Datasets were reconstructed and analyzed with the IVAS™3.6.6 software (CAMECA). The Al and Na contents were measured after background noise subtraction. Note that more than 5 samples have been investigated using TEM and APT in each condition (controlled sand casting and melt spinning). A consistent result can be obtained.

III. RESULTS

A. Controlled Sand Casting

1. The as-cast structure for the samples produced by controlled sand casting

Figure 1 shows eutectic structures observed by optical microscopy at a low magnification. Either 19 ppm (Figure 1(b)) or 160 ppm (Figure 1(c)) Na addition results in a very good modification on the eutectic Si, when compared with Al-5Si alloy (Figure 1(a)). In both cases, eutectic Si appears as a fine fibrous morphology. Due to the very similar modified eutectic Si microstructure, further characterization investigations (TEM and APT) mainly focus on the sample with the 160 ppm Na addition.

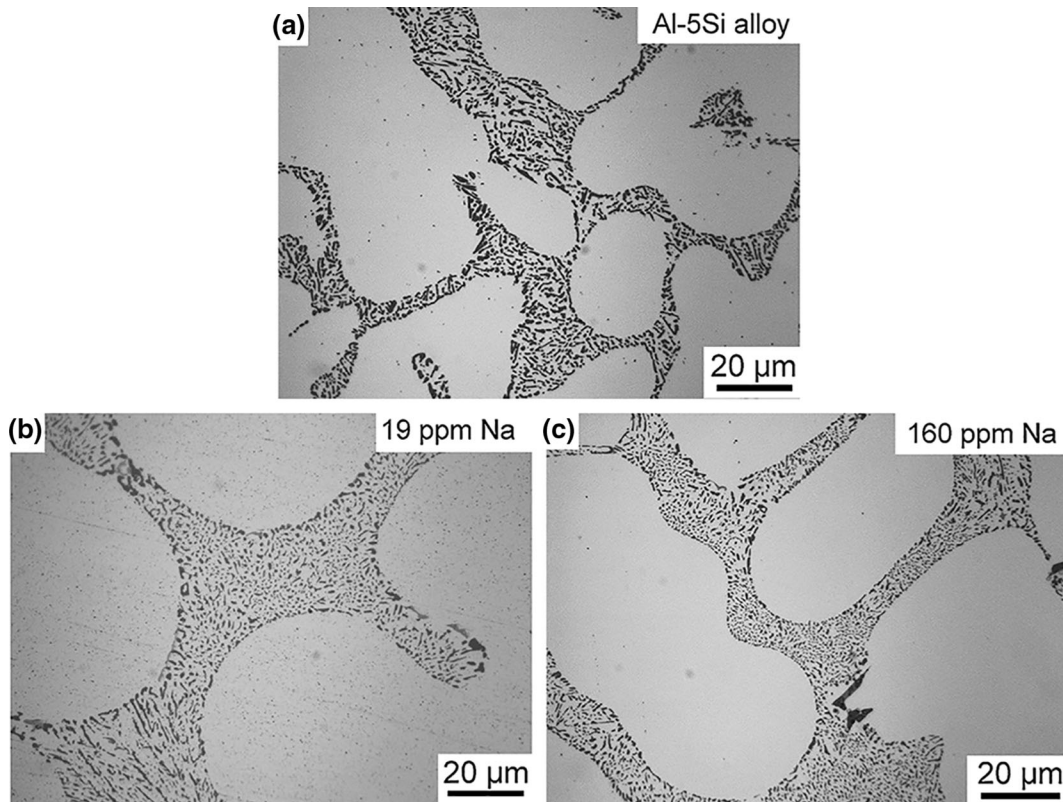


Fig. 1—The as-cast microstructures observed by optical microscopy in Al-5Si-based alloys, (a) without Na addition, (b) with 19 ppm Na addition, and (c) with 160 ppm Na addition.

2. TEM observation for the samples produced by controlled sand casting

Figure 2(a) shows two Si particles in Al-5Si alloy with 160 ppm Na addition. One Si particle (top) was tilted to the principal twinning orientation of Si ($\langle 110 \rangle_{\text{Si}}$, Figure 2(b)) to observe Si twinning. The Si particle was multiply twinned. The twinning plane is $\{111\}_{\text{Si}}$. The weaker reflections can be attributed to the double diffraction of Si caused by the multiply Si twins, as reported in Reference 7. When the Si particle was tilted to $\langle 112 \rangle_{\text{Si}}$ (Figure 2(d)), which is the typical Si growth direction according to TPPE, the Si twins appear to be not very sharp, as shown in Figure 2(c), when compared with Figure 2(a), viewed from $\langle 011 \rangle_{\text{Si}}$. However, the zig-zag geometry and the growth steps were clearly observed.

Figure 3 shows another Si particle in Al-5Si alloy with 160 ppm Na addition. Multiple Si twins with a high density were observed, as shown in Figure 3(a). Typical multiple Si twins are enlarged in Figure 3(b). Structural defects that can be correlated to Na-rich clusters appear

to be present along the $\langle 112 \rangle_{\text{Si}}$ growth direction of Si and at the intersection of two $\{111\}_{\text{Si}}$ twins, as marked with a white arrow in Figure 3(b). However, it should be noted that no further STEM-HAADF image was taken because of the very close atomic number Z ($Z_{\text{Na}} = 11$, $Z_{\text{Al}} = 13$, $Z_{\text{Si}} = 14$) and thereby the weak contrast in STEM-HAADF image. Instead, APT was employed to elucidate the distribution of Na atoms within eutectic Si.

3. APT observation for the samples produced by controlled sand casting

In order to further elucidate the distribution of Na atoms within eutectic Si, APT was performed in the bulk samples produced by controlled sand casting. Since APT analysis for such investigation is very time consuming, only one composition was analyzed; however, it is expected a similar distribution of Na in the eutectic Si phase can be observed for both compositions (19 and 160 ppm). Figure 4(a) shows an elemental map of eutectic Si in Al-5Si alloy with 160 ppm Na addition. Magnifications of three different clusters enriched in Al

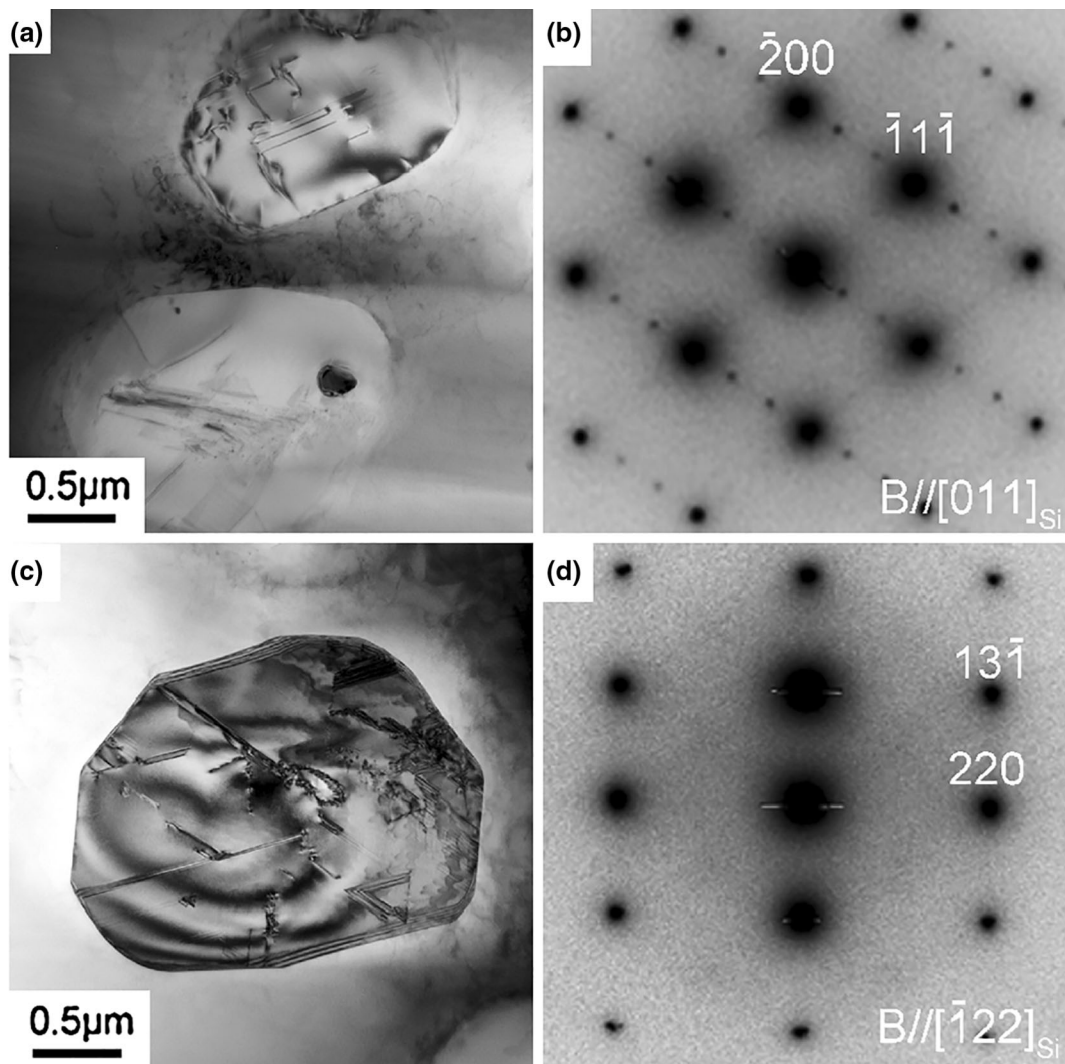


Fig. 2—(a) TEM bright field image, (b) corresponding $[011]_{\text{Si}}$ selected area diffraction pattern (SADP), (c) TEM bright field image, (d) corresponding $[112]_{\text{Si}}$ SADP, taken from Al-5Si alloy with 160 ppm Na addition.

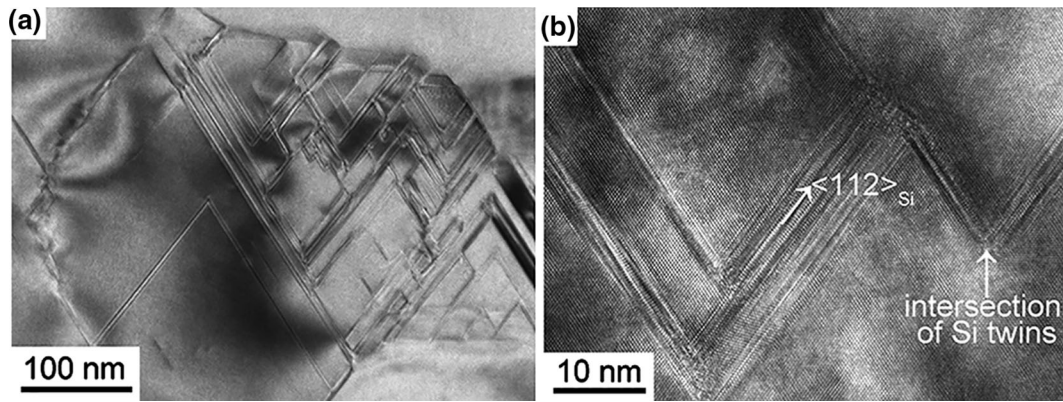


Fig. 3—(a) TEM bright field image, (b) high-resolution TEM image taken from Al-5Si alloy with 160 ppm Na addition. The beam is parallel to $[011]_{\text{Si}}$.

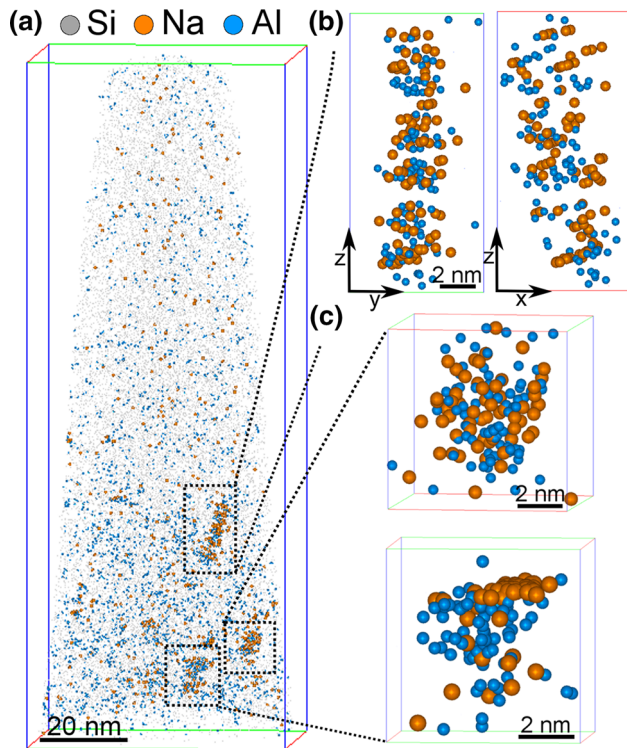


Fig. 4—Atom probe tomography of eutectic Si in Al-5Si alloy with 160 ppm Na addition, (a) complete 3D reconstruction of the data (atoms of each element are shown in different sizes for visualization purposes), (b) magnified image of a rod-like cluster, (c) magnified images of two particle-like clusters.

and Na are presented in Figures 4(b) and (c). Figure 4(b) shows two views of an elongated rod-like cluster with a size of about $4 \times 6 \times 16$ nm. Totally, 99 Al atoms and 92 Na atoms were detected in the elongated rod-like cluster. The ratio of Al:Na is close to 1. Figure 4(c) shows two round particle-like clusters with a diameter of about 4 to 6 nm. Within one round particle-like cluster, about 75 Al atoms and 51 Na atoms were detected, while, in the other round particle-like cluster, about 75 Al and 53 Na atoms were

detected. The ratio of Al:Na in these two round particle-like clusters is close to 1.5. Reporting the amount of detected atoms is preferred in contrast to concentrations, because of the small amount of atoms involved in the clusters and the difficulty of setting a region of interest to measure the concentrations. It should be noted that only about 37 pct of the total atoms in the sample can be detected in the APT instrument used.^[22] Therefore, the number of atoms reported here should not be regarded as the total amount of each species in the clusters. However, the ratio of Al and Na atoms remains unchanged.

Figure 5(a) shows an elemental map of eutectic Al and eutectic Si in the Al-5Si alloy with 160 ppm Na addition. Figure 5(b) highlights an elongated rod-like cluster in the eutectic Si, which extends up to the interface between eutectic Al and eutectic Si. Within the elongated rod-like cluster, Al and Na atoms were observed along one atomic monolayer (z - y view). When the cropped volume is viewed from another direction (x - y view), the Al and Na atoms are seen to extend over an area of approximately 4×30 nm². Figure 5(c) shows only the Na atoms in the reconstruction. A clear enrichment of Na at the interface between eutectic Al and eutectic Si was detected. For a quantitative analysis, a concentration profile at the interface between eutectic Si and eutectic Al was performed by a proximity histogram, which is constructed on an Al iso-concentration surface. An iso-surface value of 50 at. pct Al was chosen (iso-surface not shown here). Figure 5(d) shows an enrichment of ~ 0.25 at. pct Na along the interface.

The enrichment of Na seems to be slightly displaced toward the eutectic Al phase (Figure 5(d)); however, this is most probably an artifact in the APT measurement. It is theoretically known that Al atoms evaporate at a lower field than Si during APT acquisition (19 V nm^{-1} at 77 K (-196°C) for Al and 33 V nm^{-1} at 77 K (-196°C) for Si^[23]). This results in a slightly higher field evaporation rate of Al than Si during measurement. Therefore, for such spatial configurations of two phases with different values of evaporation field within the specimen, a step in the surface morphology of the specimen curvature is formed at the interface. A

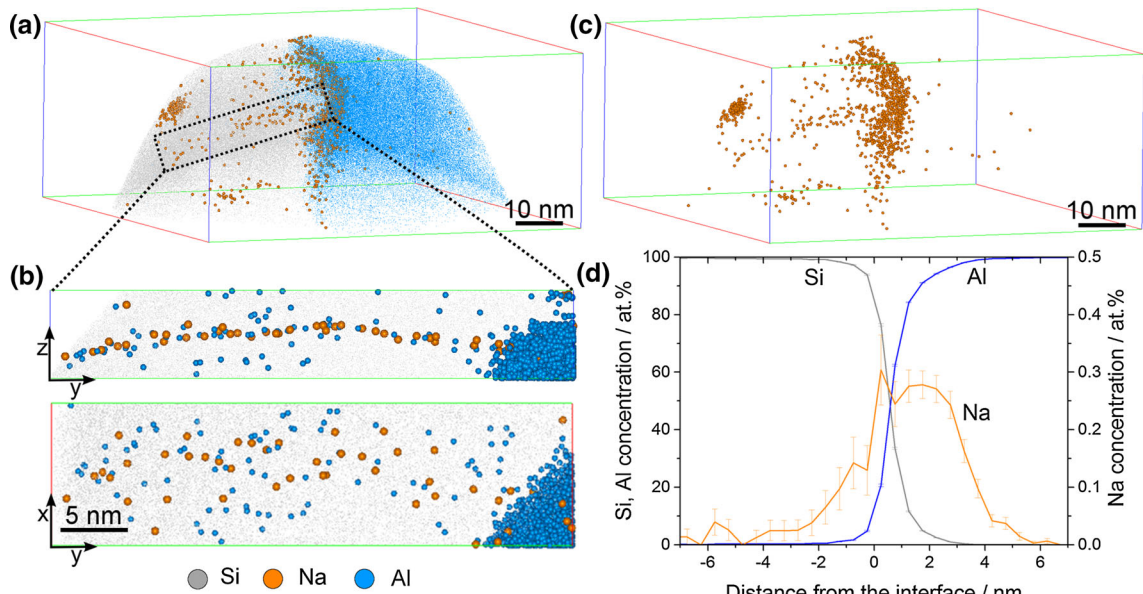


Fig. 5—Atom probe tomography of eutectic Al and eutectic Si in Al-5Si alloy with 160 ppm Na addition, (a) complete 3D reconstruction of the data with Na atoms represented as sphere, (b) a sub-volume highlighting a rod-like cluster composed of an atomic monolayer, (c) atomic map of Na atoms showing Na enrichment at the interface between eutectic Al and eutectic Si, (d) concentration profile across the interface constructed using proximity histogram, showing the enrichment of Na at the interface.

slight morphological change along an interface may lead to broadening of segregated elements at the interface as a result of ion-trajectory aberrations. A recent field evaporation simulation by C. Oberdorfer *et al.*^[24] explains such effects in detail.

B. Entrained Si After Melt Spinning and DSC

1. DSC

Figure 6 shows a DSC trace taken from Al-5Si alloys produced by controlled sand casting. Only the eutectic Si [about 850 K (577 °C)] was reflected in DSC curve. It is not possible to investigate the nucleation of eutectic Si using DSC analyses for the samples produced by controlled sand casting. Therefore, no further detailed investigation was performed. In contrast, Figure 7 shows DSC traces taken from Al-5Si alloys without (Figure 7(a)) and with 19 ppm Na (Figure 7(b)) and 160 ppm Na (Figure 7(c)) additions, respectively. Two distinct solidification exotherms were observed. The first exotherm corresponds to the solidification of the eutectic Si along the grain boundaries.^[6] The second exotherm is associated with the solidification of entrained eutectic droplets embedded in the α -Al matrix. The undercooling of the entrained eutectic droplets (ΔT) was defined as the difference between the onset temperatures of these two exotherms. Therefore, only the onset temperatures are marked in Figure 7. The peak temperature is very helpful to elucidate the nucleation kinetics at different cooling rates (DSC heating and cooling rates). However, in the present manuscript, only one cooling rate (10 K min^{-1}) was used. Therefore, no further analysis on the peak temperature is included here. The entrained eutectic undercooling can be obtained reliably with a reproduction of about 0.2 K

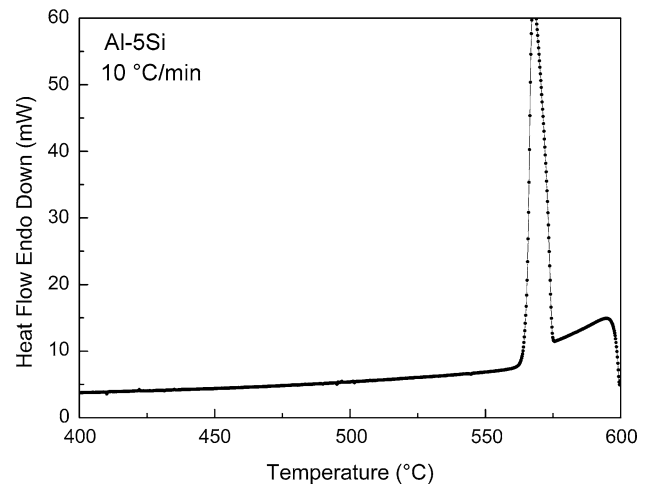


Fig. 6—DSC solidification exotherms of Al-5Si alloy produced by controlled sand casting at a cooling rate of 10 K min^{-1} (10 °C min^{-1}).

to 0.5 K (0.2 °C to 0.5 °C). In the case of Al-5Si alloy without Na addition, the measured undercooling of the entrained eutectic droplets (ΔT) is about 24 K (24 °C), as shown in Figure 7(a). In the case of Al-5Si alloy with 19 ppm Na addition, the measured undercooling of the entrained eutectic droplets (ΔT) is about 49 K (49 °C). Clearly, 19 ppm Na addition does lead to a significant depression on the nucleation of entrained eutectic droplets. However, further increasing Na addition up to 160 ppm decreases the undercooling [29 K (29 °C)]. Furthermore, it should be noted that the second exotherm in Na-containing samples (Figures 7(b), (c)) is much wider than that of Na-free sample (Figure 7(a)),

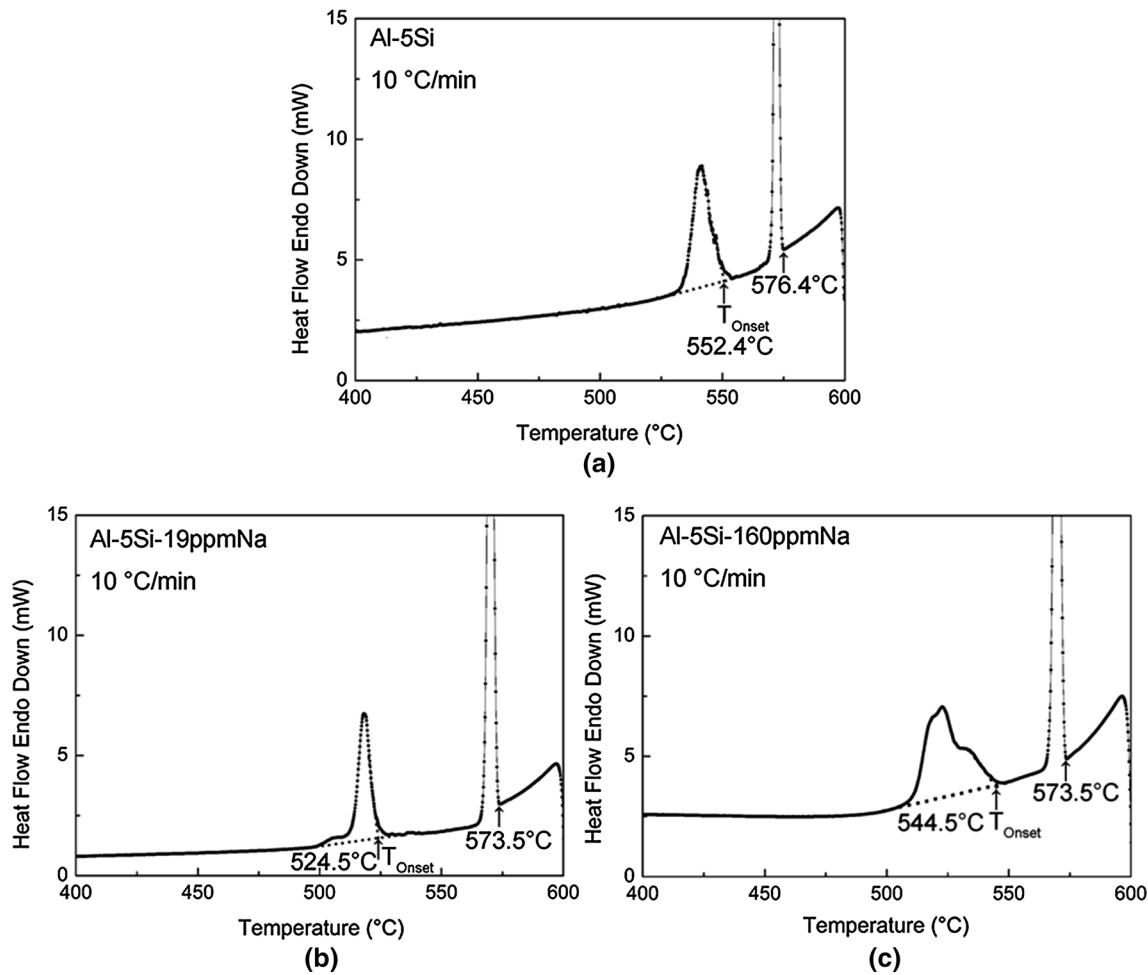


Fig. 7—DSC solidification exotherms of melt spun Al-5Si alloys without Na addition (a) and with 19 ppm Na (b), 160 ppm Na (c) additions at a cooling rate of 10 K min^{-1} ($10 \text{ }^\circ\text{C min}^{-1}$).

indicating a wider size distribution of the entrained eutectic droplets.^[6] Such typical observation is always present after four DSC runs, as shown in Figure 8. However, it should be pointed out that the shape of the second exotherm has no significant effect on the measurement of the entrained eutectic undercooling because the entrained eutectic undercooling is measured using the onset temperature of the exotherms.

2. TEM observation for the samples produced by melt spinning

Similar to the case of the controlled sand casting, TEM characterization mainly focuses on the sample with the 160 ppm Na addition. Figure 9 shows a TEM bright field image of two Si particles in melt spun Al-5Si alloy with 160 ppm Na addition. Parallel Si twins (left Si particle) and multiple Si twins (right Si particle) were observed, as shown in Figure 9(a), and can be seen more clearly in Figures 10(b) and (c). The parallel Si twins can be interpreted according to TPRES growth mechanism, while multiple Si twins can be interpreted according to IIT growth mechanism. The TPRES growth mechanism

appears to form a much finer twin structure in the $\langle 112 \rangle_{\text{Si}}$ directions respective facets in the case of melt spinning, when compared with the case of controlled sand casting (Figure 3(a)). However, no or little change of directions was observed. In contrast, the IIT growth mechanism appears not to provide such a fine structure but facilitates a change of growth direction in non-constrained solidification conditions. This is fully consistent with the TEM observation in the case of controlled sand casting (Figures 2, 3). Furthermore, the number density of Si twins in melt spun condition appears to be much higher due to the high cooling rates during melt spinning.

Several APT attempts have also been made to measure the Na distribution in melt spun samples. However, melt spun samples have an extremely fine Si structure which makes site-specific sample preparation for APT very challenging. Although further APT measurement is still required for melt spun samples, a similar Na distribution can be expected in both samples produced by melt spinning and controlled sand casting.

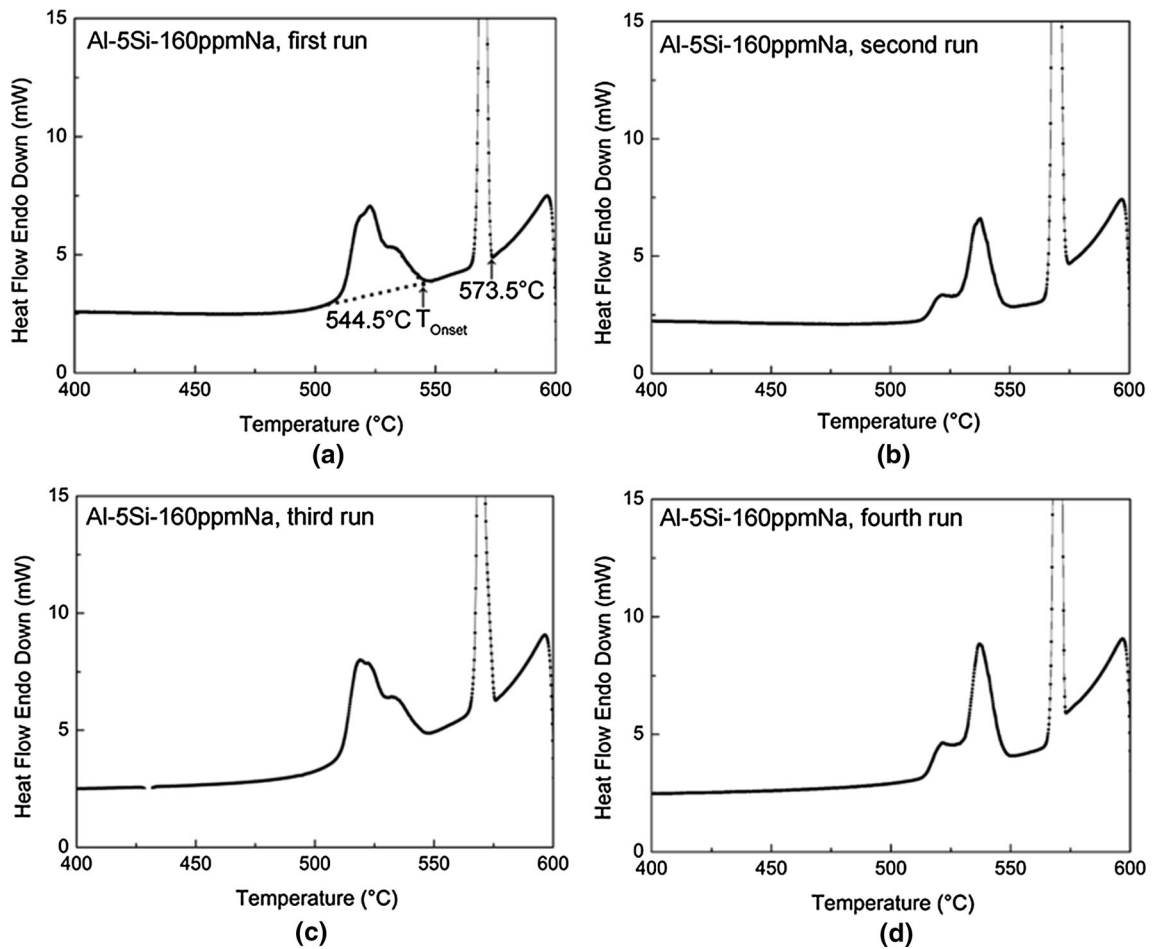


Fig. 8—DSC solidification exotherms of melt spun Al-5Si alloys with 160 ppm Na addition after the first (a), second (b), third (c), and fourth (d) DSC run at a cooling rate of 10 K min^{-1} ($10 \text{ }^\circ\text{C min}^{-1}$).

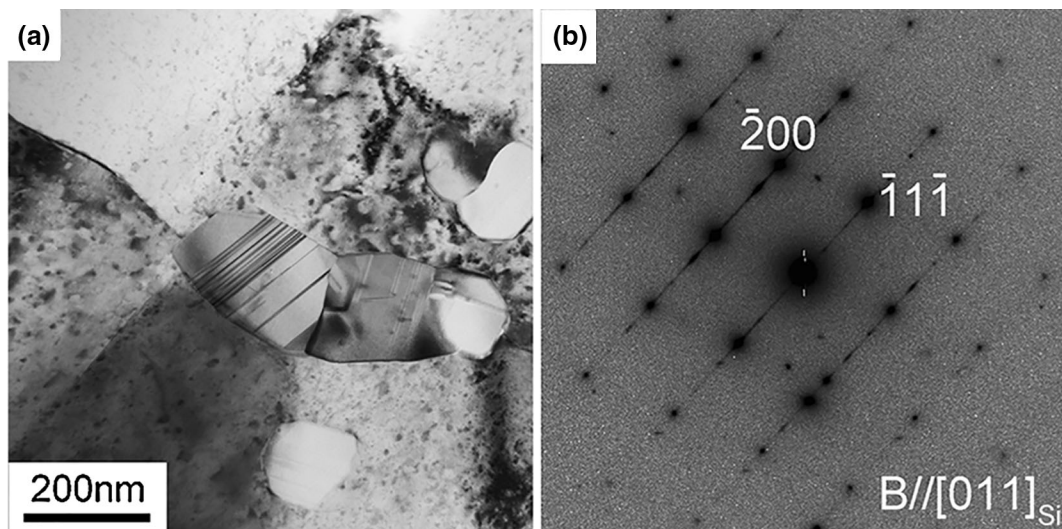


Fig. 9—(a) TEM bright field image, (b) corresponding $[011]_{\text{Si}}$ SADP of Si particles taken from melt spun Al-5Si alloy with 160 ppm Na addition. The beam is parallel to $[011]_{\text{Si}}$.

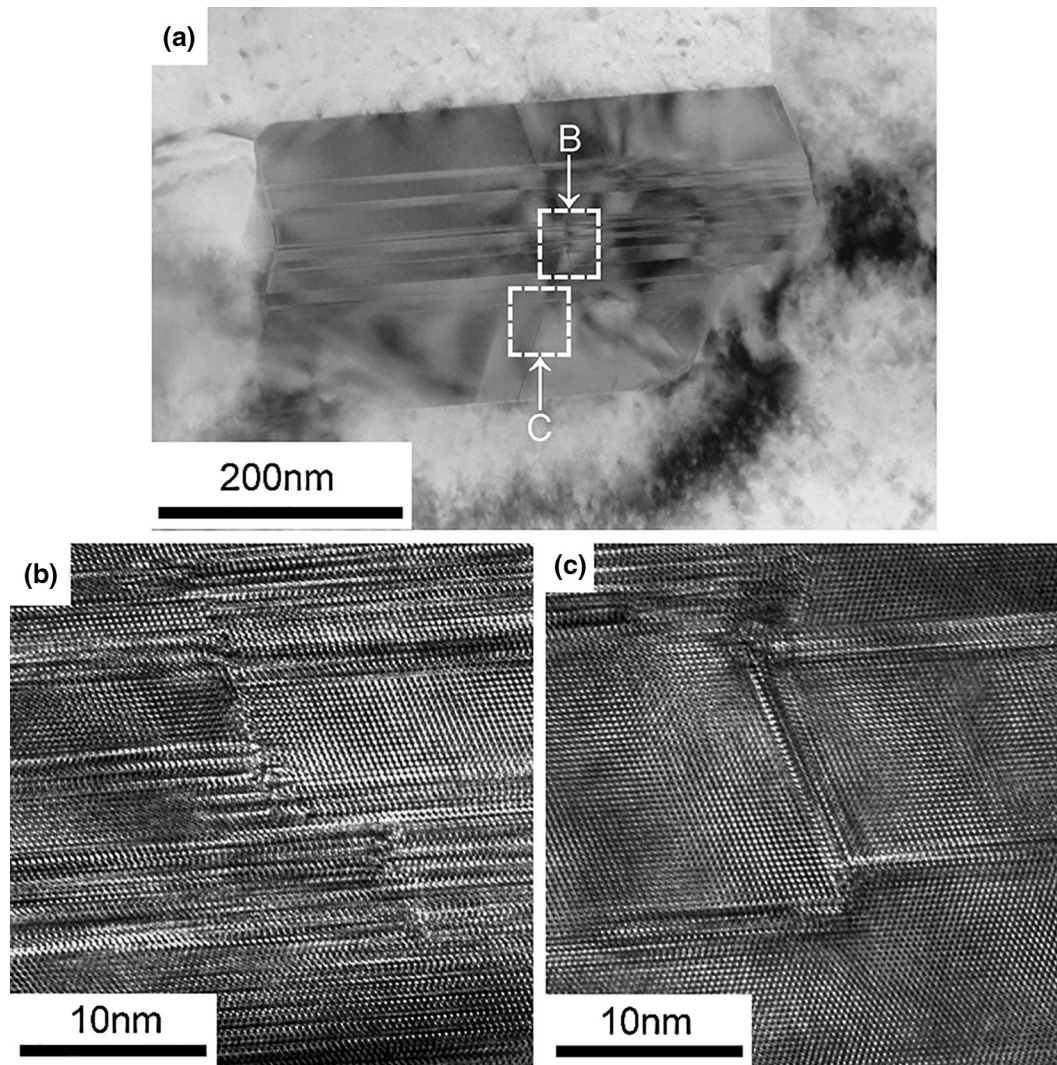


Fig. 10—(a) TEM bright field image of a multiple twinned Si particle taken from melt spun Al-5Si alloy with 160 ppm Na addition. (b), (c) are enlarged from the areas as marked with white boxes ((B) and (C) in (a), respectively, showing Si twinning. The beam is parallel to $[011]_{\text{Si}}$.

IV. DISCUSSION

A. Growth of Eutectic Si

In terms of the growth of eutectic Si, 160 ppm Na addition into Al-5Si alloy promotes significant Si twins both in the cases of controlled sand casting (Figures 2, 3) and melt spun condition (Figures 9, 10), respectively. This is very similar to the case of Sr addition, indicating that the modification mechanism can be interpreted in a similar way. As reported in Reference 7, the twin density (*i.e.*, number of twins per length) can be evaluated by counting the number of the twins intersecting a perpendicular reference line. An analysis of at least ten twinned Si particles in melt spun Al-5Si-based alloy yields an average twin density of about $1.6 \pm 0.4 \times 10^{-4} \text{ nm}^{-1}$. In contrast, a total analysis of at least ten twinned Si particles in Al-5Si-based alloy with 160 ppm Na addition provides a value of $4.8 \pm 0.85 \times 10^{-2} \text{ nm}^{-1}$ for the average twin density, which is two orders of magnitude higher than that of melt spun Al-5Si-based alloy,

strongly indicating that 160 ppm Na addition indeed promotes significant Si twins.

For the first time, the adsorption of Na atoms within eutectic Si was clearly observed by APT. The elongated rod-like clusters and round particle-like clusters were found to be enriched with Al and Na atoms, which are fully consistent with the previous report^[19] using STEM X-ray elemental mapping that Na is localized in small particles, rather than being adsorbed uniformly in the eutectic Al or eutectic Si. Although no detailed structural information (*i.e.*, orientations) of such types of clusters can be easily extracted from APT data, the elongated rod-like clusters can be proposed to be oriented along the $\langle 112 \rangle_{\text{Si}}$ growth direction of Si when correlated to the high-resolution TEM image (Figure 3(b)). Indeed, the length (about 20 nm, Figure 3(b)) and the width (about 2 to 3 nm, Figure 3(b)) of Si twins observed by TEM are very close to that of the elongated rod-like cluster ($4 \times 6 \times 16 \text{ nm}$) observed by APT. The round particle-like clusters can be proposed to be

located at the intersection of the two $\{111\}_{\text{Si}}$ twins when the APT and high-resolution TEM image (Figure 3(b)) are compared.

The difference of cluster types can be further supported by the fact that the ratio of Al:Na (1.5) within the round particle-like clusters is higher than that (1) within the elongated rod-like clusters, strongly indicating that a possible different segregation pattern may occur. It should be noted here that, from TEM images, the crystallographic orientation and location of TPRES mechanism are identical to that of the IIT mechanism and cannot be differentiated by the crystallography alone because the intersection of Si twins for IIT and the corner for TPRES appear as single points, when viewed in $\langle 011 \rangle_{\text{Si}}$ direction. However, from APT, the IIT segregation pattern appears to be round particle-like clusters enriched with Al, Si, and Na atoms, while the poisoning of the TPRES segregation pattern appears to be elongated rod-like clusters or segregation line along the $\langle 112 \rangle_{\text{Si}}$ growth direction of Si enriched with Al, Si, and Na atoms (Figures 4(b), 5(b)). For clarity, two types of the segregation patterns within eutectic Si, corresponding to poisoning of the TPRES and IIT segregation patterns, are marked in Figures 11(a) and (b), respectively.

The elongated rod-like clusters result as a segregation pattern of the poisoning of the TPRES mechanism. Na atoms are adsorbed at the TPRES hindering growth but are quickly overgrown by subsequent Si growth on $\{111\}_{\text{Si}}$ facets. Excess Al can segregate out ahead of the growing interface, as marked with a red arrow in Figure 11(a), leading to lower Al concentrations in the elongated rod-like clusters. The round particle-like clusters can be related to the multiple IIT events on $\{111\}_{\text{Si}}$ facets. When newly formed $\{111\}_{\text{Si}}$ facets grow subsequent to the IIT event, a secondary IIT of Na atoms may occur on these $\{111\}_{\text{Si}}$ facets, as marked with dashed Na atoms in Figure 11(b). Subsequently, these $\{111\}_{\text{Si}}$ facets grow toward each other and entrap the solute-rich diffusion fields ahead of the $\{111\}_{\text{Si}}$ facets. Once entrapped, the liquid has no path for Al to segregate out, and thereby higher Al concentration was observed in the round particle-like clusters. The entrapped liquid itself forms clusters, which can be caused

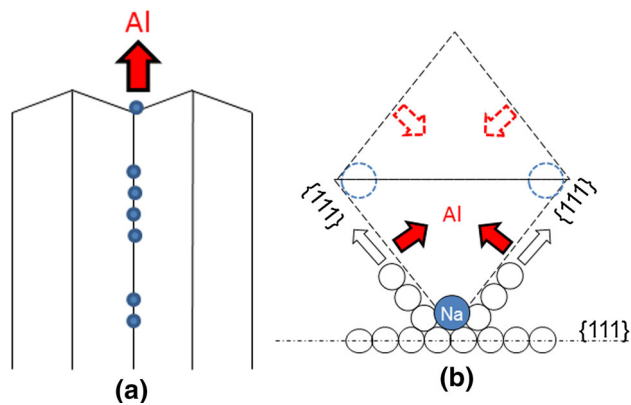


Fig. 11—Schematic representation of the adsorption of Na atoms along the $\langle 112 \rangle_{\text{Si}}$ growth direction of Si (poisoning of the TPRES) (a) and at the intersection of Si twins (IIT) (b) within eutectic Si.

by the surface minimization and ripening exhibiting a more spherical morphology.

Comparing the information collected from the high-resolution experimental analysis with the IIT and poisoning of the TPRES growth mechanism, one question arises how Na atoms are adsorbed on $\{111\}_{\text{Si}}$ growth planes. It is still not clear whether the Na adsorption occurs within one monolayer. The adsorption of Na atoms was observed within one monolayer, as shown in Figure 5(b). Although, viewed from the other direction (x - y view), Al and Na atoms were observed to extend over an area of approximately $4 \times 30 \text{ nm}^2$, this planar monolayer of Na and Al atoms can be therefore assumed to correspond to a region of narrow twins, as shown in Figure 3(b). Thus, it can be proposed that only one monolayer of Na atoms can induce the poisoning of the TPRES growth mechanism. The Na-rich segregation line (Figure 5(b)) is indicative of the repeated poisoning of the TPRES growth mechanism. Similarly, the adsorption of Na atoms within one monolayer at the intersection of two $\{111\}_{\text{Si}}$ twins can also induce the IIT growth mechanism. The formation of Na-rich clusters with different compositions and morphologies can be attributed to the continuous solute segregation and entrapment of Al, Si, and Na atoms during continuous Si growth. Further detailed discussion on the solute adsorption and entrapment has been made elsewhere.^[25]

The adsorption of Na atoms at the interface between Al and Si was also clearly observed, as shown in Figure 5(c), (d). An enrichment of Na (about 0.25 at. pct) was, for the first time, measured, as shown in Figure 5(d). It should be pointed out that this observation is fully consistent with the previous report^[26] that Na atoms are rejected by the Al and Si phase during solidification because of the low solubility of Na in Al and Si. Such type of Na enrichment provides a direct experimental support to the assumption that Na atoms are segregated ahead of the solidification front and hinder the growth of eutectic Si.

B. Nucleation of Eutectic Si

In terms of the nucleation of eutectic Si, the measured entrained eutectic undercooling [24 K (24 °C)] in Al-5Si alloy is consistent with the previous report^[6] that the undercooling of Al-5Si binary alloy is about 20.5 K (20.5 °C) (4N Si) and 31 K (31 °C) (5N Si), respectively. However, given the used materials (5N Si) in the present investigation, some impurities may be present. 19 ppm Na addition does lead to a significant depression on the nucleation of entrained eutectic droplets in high purity Al-5Si alloy. The measured undercooling of the entrained eutectic droplets (ΔT) is about 49 K (49 °C), which is fully consistent with the previous report [about 48 K (48 °C)].^[19] However, a decreased undercooling [29 K (29 °C)] was observed in the case of 160 ppm Na addition, indicating that the nucleation kinetic of entrained eutectic Si may be related to the Na content.

According to the calculation of the required Na to form the Na_3P phase instead of AlP ,^[19] about two times of the Na content (e.g. $c_{\text{Na}} = 2c_p$, 0.88 ppm) are needed

to fully react with the P (0.44 ppm, Table I). 19 or 160 ppm Na addition in the present investigation is sufficient to completely remove the effect of P on the nucleation of eutectic Si. However, this is not the case. The undercooling does not further reduce with increasing Na content, indicating that the nucleation mechanism may be not simply due to the formation of Na₃P phase. The solubility of Na atoms in eutectic Al and eutectic Si should be taken into consideration, as suggested in Reference 19. Following discussion will be made in terms of the remaining AIP phase, which can form AIP patches to nucleate Si.

As to the remaining AIP phase, it has been reported^[6,27] that the Gibbs free energy (ΔG) of the Na₃P phase (−200 kJ/mol) is less than that of AIP phase (−115 kJ/mol), indicating that the Na₃P phase is thermodynamically more stable and must be preferentially formed. However, the less stable AIP phase is not fully transformed to the stable Na₃P phase because there is a competition between the stable and less stable compounds. The equilibrium reaction ($\text{AIP} \leftrightarrow \text{Al} + \text{P}$) determined the AIP available for the nucleation of eutectic Si.

Through the interaction between AIP and Na₃P phase ($\text{AIP} + 3\text{Na} \leftrightarrow \text{Na}_3\text{P} + \text{Al}$), the activity of AIP varies greatly with respect to the original concentration. Furthermore, Na content may also affect the activity of AIP. The activity of AIP can be measured by the activity coefficient. The equilibrium fraction between the competing phases establishes itself by the formula^[28,29]:

$$k_{\text{AIP}} = a_{\text{AIP}}/x_{\text{AIP}} = \frac{\text{Activity of AIP}}{\text{Real concentration of AIP}} \quad [1]$$

where a_i and k_{AIP} are the activity and activity coefficient of AIP, respectively. This formula determines the remaining AIP which can form AIP patches to nucleate eutectic Si within the droplet. However, activity (a_i) and activity coefficient (k_{AIP}) are often not known for phosphide compounds. Thus, despite the presence of more stable phosphide compounds (*i.e.*, Na₃P phase), AIP patches may still be present. Their amount could be estimated if the thermodynamic data are known.^[6] Their size or size distribution will be dependent on the adsorption kinetics such as a line tension and other factors.^[20] This argument is fully consistent with the observed undercooling of entrained eutectic droplets in the present investigation, indicating that sufficient AIP is still available for the nucleation of eutectic Si despite the presence of the sufficient Na (160 ppm). Detecting AIP particle (in the center of Si particle) is extremely challenging, due to the very low P content (about 0.44 ppm), as listed in Table I. Although it is more likely to detect such type AIP particle with higher P contents (*e.g.* 10 ppm P or higher), the present investigation focuses on the case of low P contents. Further investigation on AIP particle is still required.

V. CONCLUSIONS

1. The adsorption of Na atoms was, for the first time, observed at an atomic scale. The adsorption of Na

atoms was further proposed to occur at the intersection of multiple Si twins and along the $\langle 112 \rangle_{\text{Si}}$ growth direction of Si, which provides a strong experimental support to the IIT growth mechanism and poisoning of the TPRES growth mechanism.

2. The adsorption of Na atoms within one monolayer can induce the IIT growth mechanism and poisoning of the TPRES growth mechanism, while the formation of round particle-like Na-rich clusters at the intersection of multiply Si twins and elongated rod-like Na-rich clusters along the $\langle 112 \rangle_{\text{Si}}$ growth direction of Si can be attributed to the continuous solute segregation and entrapment of Al, Si, and Na atoms during continuous Si growth.
3. The adsorption of Na atoms was, for the first time, observed at the interface between eutectic Si and eutectic Al, which is believed to hinder the growth of eutectic Si and thereby affect its morphology.
4. 19 ppm Na addition results into a high-entrained eutectic undercooling. However, further increasing Na addition up to 160 ppm exerts no positive effects on the nucleation of eutectic Si. Instead a slight decrease of undercooling was observed. The formation of thermodynamic stable Na₃P phase was proposed to deteriorate the AIP potency in Al-Si alloys. However, the remaining AIP phase can still nucleate Si.

ACKNOWLEDGMENTS

J.H. Li gratefully acknowledges the access to TEM at the Erich Schmid Institute of Materials Science of the Austrian Academy of Sciences. The EU funding in the framework of the project AME-Lab (European Regional Development Fund C/4-EFRE-13/2009/Br) is gratefully acknowledged. The Atom Probe was financed by the DFG and the Federal State Government of Saarland (INST 256/298-1 FUGG). J. Barrirero acknowledges the Erasmus Mundus Programme of the European Commission within the Doctoral Programme DocMASE for financial support.

REFERENCES

1. A. Pacz: US Patent No. 1387900, 1921.
2. S.-Z. Lu and A. Hellawell: *Metall. Trans. A*, 1987, vol. 18A, pp. 1721–33.
3. R.S. Wanger: *Acta Metall.*, 1960, vol. 8, p. 57.
4. R.D. Hamilton and R.G. Seidensticker: *J. Appl. Phys.*, 1960, vol. 31, p. 1165.
5. M.G. Day and A. Hellawell: *Proc. R. Soc. Lond. A*, 1968, vol. 305, pp. 473–91.
6. J.H. Li, M. Zarif, M. Albu, B. McKay, F. Hofer, and P. Schumacher: *Acta Mater.*, 2014, vol. 72, pp. 80–98.
7. J.H. Li, M. Zarif, G. Dehm, and P. Schumacher: *Philos. Mag.*, 2012, vol. 92, pp. 3789–05.
8. M. Zarif, B. McKay, and P. Schumacher: *Metall. Mater. Trans. A*, 2011, vol. 42A, pp. 1684–91.
9. K. Nogita, H. Yasuda, K. Yoshida, K. Uesugi, A. Takeuchi, Y. Suzuki, and A.K. Dahle: *Scripta Mater.*, 2006, vol. 55, pp. 787–90.

10. K. Nogita, H. Yasuda, M. Yoshiya, S.D. McDonald, K. Uesugi, A. Takeuchi, and Y. Suzuki: *J. Alloys Compd.*, 2010, vol. 489, pp. 415–20.
11. M. Timpel, N. Wanderka, R. Schlesiger, T. Yamamoto, N. Lazarev, D. Isheim, G. Schmitz, S. Matsumura, and J. Banhart: *Acta Mater.*, 2012, vol. 60, pp. 3920–28.
12. M. Timpel, N. Wanderka, R. Schlesiger, T. Yamamoto, D. Isheim, G. Schmitz, S. Matsumura, and J. Banhart: *Ultramicroscopy*, 2013, vol. 132, pp. 216–21.
13. J. Barrirero, M. Engstler, N. Ghafoor, N. de Jonge, M. Odén, and F. Mücklich: *Alloys Compd.*, 2014, vol. 611, pp. 410–21.
14. M. Faraji and L. Katgerman: *Micron.*, 2010, vol. 41, pp. 554–59.
15. Q.Y. Liu, Q.C. Li, and J.R. Zhang: *Scripta Metall.*, 1988, vol. 22, pp. 789–91.
16. K. Kobayashi, P.H. Shingu, and R. Ozaki: *J. Mater. Sci.*, 1975, vol. 10, pp. 290–99.
17. Y.H. Cho, H.C. Lee, K.H. Oh, and A.K. Dahle: *Metall. Mater. Trans. A*, 2008, vol. 10A, p. 2435.
18. P.B. Crosley and L.F. Mondolfo: *Mod. Cast.*, 1966, vol. 49, p. 63.
19. C.R. Ho and B. Cantor: *J. Mater. Sci.*, 1995, vol. 30, pp. 1912–20.
20. C.R. Ho and B. Cantor: *Acta Metall. Mater.*, 1995, vol. 43, pp. 3231–46.
21. K. Thompson, D. Lawrence, D.J. Larson, J.D. Olson, T.F. Kelly, and B. Gorman: *Ultramicroscopy*, 2007, vol. 107, pp. 131–39.
22. T.F. Kelly and M.K. Miller: *Rev. Sci. Instrum.*, 2007, vol. 78, p. 031101.
23. M.K. Miller: *Atom Probe Tomography: Analysis at the Atomic Level*, Kluwer Academic/Plenum, New York, 2000.
24. C. Oberdorfer, S.M. Eich, and G. Schmitz: *Ultramicroscopy*, 2013, vol. 128, pp. 55–67.
25. J.H. Li, M. Albu, F. Hofer, and P. Schumacher: *Acta Mater.*, 2015, vol. 83, pp. 187–202.
26. L. Clapham and R.W. Smith: in *Partitioning of Strontium Modifier to Individual Phases in Al-Si Eutectic*, J. Beech and H. Jones, eds., *Proc. 4th Decenn. Int. Conf. Solidif. Process*, Sheffield, 1987.
27. M.E. Schlesinger: *Chem. Rev.*, 2002, vol. 102, pp. 4267–4301.
28. D.A. Porter, K.E. Easterling, and M.Y. Sherif: *Phase Transformation in Metals and Alloys*, 3rd ed., CRC Press, Boca Raton, FL, 2009.
29. E.B. Smith: *Basic Chemical Thermodynamics*, 4th ed., Oxford University Press, New York, NY, 1990.